

Generative AI-Based Probabilistic Constellation Shaping With Diffusion Models

Mehdi Letafati, *Student Member, IEEE*, Samad Ali, *Member, IEEE*, and Matti Latva-aho, *Senior Member, IEEE*

Abstract—Diffusion models are at the vanguard of generative AI research with renowned solutions such as ImageGen by Google Brain and DALL.E 3 by OpenAI. Nevertheless, the potential merits of diffusion models for communication engineering applications are not fully understood yet. In this paper, we aim to unleash the power of generative AI for PHY design of constellation symbols in communication systems. Although the geometry of constellations is predetermined according to networking standards, e.g., quadrature amplitude modulation (QAM), probabilistic shaping can design the probability of occurrence (generation) of constellation symbols. This can help improve the information rate and decoding performance of communication systems. We exploit the “denoise-and-generate” characteristics of denoising diffusion probabilistic models (DDPM) for probabilistic constellation shaping. The key idea is to learn generating constellation symbols out of noise, “mimicking” the way the receiver performs symbol reconstruction. This way, we make the constellation symbols sent by the transmitter, and what is inferred (reconstructed) at the receiver become as similar as possible, resulting in as few mismatches as possible. Our results show that the generative AI-based scheme outperforms deep neural network (DNN)-based benchmark and uniform shaping, while providing *network resilience* as well as *robust out-of-distribution performance* under low-SNR regimes and non-Gaussian assumptions. Numerical evaluations highlight 30% improvement in terms of cosine similarity and a threefold improvement in terms of mutual information compared to DNN-based approach for 64-QAM geometry.

Index Terms—AI-native wireless, constellation shaping, diffusion models, generative AI, network resilience, wireless AI.

I. INTRODUCTION

With the incredible results achieved from generative pre-trained transformers (GPT) and diffusion models, generative AI is envisioned to be at the forefront of technological advancements in various industrial and academic domains [2]–[4]. In the vanguard of generative AI research, diffusion models have showcased outstanding performance with renowned solutions such as ImageGen,¹ DALL.E 3,² and stable diffusions,³ to name a few [5]. In parallel, the future generations of wireless systems entail the extensive integration of AI and machine learning (AI/ML) algorithms into the

communication and networking design, realizing “AI-native” wireless networks [6]–[10]. This highlights the necessity for developing novel AI/ML solutions that are tailored to address the requirements of emergent communication scenarios.

The majority of the research carried out thus far on AI-native communication and signal design, has primarily concentrated on “discriminative” AI/ML models [11]–[14]. The objective of such models is to simply learn the “boundaries” between classes or latent spaces within high-dimensional signals. In contrast, “generative” models essentially learn the *representations* of highly-structured signals and generate desired samples accordingly. Inspired by the insights provided in [3] for WiGenAI (a new vision on generative AI-based wireless system design), our goal in this paper is to unleash the power of generative AI at the transmitter of wireless systems, by proposing diffusion-based probabilistic constellation shaping. *To the best of our knowledge, this is the first technical paper that proposes diffusion models for the application of PHY signal design in wireless communications.*

A. Literature Review

Despite the fact that remarkable results have been achieved by diffusion models in various domains of computer science, such as natural language processing (NLP) [15], computer vision [16], molecule generation [17], and medical imaging [18], there are only a few papers in communication literature that have studied the applications of diffusion models for wireless systems [19]–[23].

In [19], diffusion models are employed at the receiver of a communication system for image transmission, as a complement for deep learning-based joint source-channel coding scheme. The goal is to progressively refine the image at the receiver, taking the perception-distortion trade-of into account. Considering a similar objective within a similar application, the authors in [20] combine diffusion models and invertible neural networks for high-quality source image recovery. The results highlight a perceptual improvement in the reconstruction performance under low bandwidth and low signal-to-noise ratio (SNR) conditions, compared to the deep learning-based approaches. As another hybrid approach, [21] employs diffusion models to improve the receiver’s performance in terms of channel estimation error removal. Although diffusion models have shown promising performance in removing noise components and reconstructing data samples, the authors employ an additional autoencoder block. However, implementing two different ML models, each with a distinct objective function can impose computational overhead to the network. Furthermore, the output signals of the employed

This work has been submitted to the IEEE for possible publication. Copyright may be transferred without notice, after which this version may no longer be accessible.

Preliminary results of this paper are submitted to the IEEE International Conference on Machine Learning for Communication and Networking (ICMLCN 2024), Stockholm, Sweden, May 2024 [1].

The authors are with the Centre for Wireless Communications, University of Oulu, Oulu, Finland (e-mails: mehdi.letafati@oulu.fi; samad.ali@oulu.fi; matti.latva-aho@oulu.fi).

¹<https://imagen.research.google/>

²<https://openai.com/dall-e-3>

³<https://github.com/CompVis/latent-diffusion>

encoder part does not necessarily follow the standard format of constellation symbols, making the scheme inapplicable to real-world wireless systems. Score-based diffusion models are employed in [22] for channel estimation in multi-input-multi-output (MIMO) wireless communications. RefineNet neural architecture [24], comprised of 24 hidden channels in the first layer and a depth of six residual blocks in both the encoder and decoder parts, is implemented to estimate the gradient of the log-prior of wireless channels. The results imply a competitive performance of diffusion models for both in-distribution and out-of-distribution (OOD) scenarios compared to generative adversarial network (GAN). In a recent work [23], we have proposed exploiting diffusion models for a hardware-impaired communication system, showcasing more than 25 dB improvement in reconstruction performance compared to deep neural network (DNN)-based receivers.

B. Our Work

With the aid of generative AI, particularly diffusion models, our goal in this paper is to take a step towards a generative AI-native system, in which we can continuously design radio signals, adapt to changes, and realize “reciprocal understanding” between communication parties. To this end, we propose denoising diffusion probabilistic models (DDPM), as one of the state-of-the-art generative models proposed by Ho *et al.* in 2020 [25], for probabilistic constellation shaping at the transmitter. To the best of our knowledge, this is the first paper that proposes diffusion models for constellation shaping in communication systems.

The motivation behind our work is that the choice of constellations can significantly affect the performance of communication systems. Recently, deep learning techniques are proposed for geometric shaping [26]–[28]. They typically employ “discriminative” models, particularly classical autoencoders, and let the neural model decide about the constellation symbols for transmission. This results in arbitrary forms of constellation points that might not be compliant with wireless standards such as the 3rd Generation Partnership Project (3GPP) [29]. To overcome this challenge, probabilistic constellation shaping can be employed—it designs the probability of occurrence (generation) of constellation symbols within the corresponding geometry, aiming to enhance the information rate and decoding performance of communication systems. Unlike previous works that try to deal with the optimization of discrete distributions [28], we offer a radically different approach and exploit the “denoise-and-generate” characteristic of DDPMs for probabilistic shaping.

In our proposed scheme, a DDPM is first trained with the goal of learning the diffusion process for generating constellation symbols. Within each transmission slot, the transmitter runs the diffusion model to probabilistically shape (generate) the constellation symbols according to the signal-to-noise ratio (SNR) level. Intuitively, the goal is to do shaping in a way that the information-bearing constellation symbols generated at the transmitter, and what is inferred (reconstructed) at the receiver become as similar as possible, resulting in as few mismatches between the communication

parties as possible. The key idea to fulfill this requirement is that we exploit the “denoise-and-generate” characteristic of DDPMs to help communication parties maintain “reciprocal understanding” of how to map and demap the information symbols according to the noise level (or equivalently the channel SNR) of the communication link over time. More details of our proposed approach are provided in Section III. Previous works require both the transmitter and the receiver to get involved in the “joint” training of the system by passing the loss function gradient [26], [28] (or its approximation [12]) through the channel layers. This might cause some incompatibility issues between the transmitter (e.g., the base station of a cellular network from a specific vendor) and the receiver (e.g., a user equipment from another vendor). Nevertheless, our approach requires only one neural model which is pre-trained and identically employed by both of the communication parties within a diffusion-based framework.

Through extensive numerical experiments, we show that our proposed approach outperforms DNN-based scheme with trainable constellation layer and neural demapper [28]. Notably, we show that 30% improvement in terms of cosine similarity and a threefold improvement in terms of mutual information are achieved compared to DNN-based solution for 64-QAM geometry and 0 dB SNR. Our results also highlight that the proposed DDPM-based scheme is *resilient* against low-SNR regimes. We also study the *out-of-distribution (OOD) performance* of our scheme under non-Gaussian assumptions. Furthermore, we compare our probabilistic shaping scheme with uniform shaping baseline, and show that the proposed DDPM achieves a notable performance compared to the conventional uniform shaping as well.

C. Paper Organization and Notations

In what follows, we first introduce the framework of DDPM, together with the main formulas and the corresponding loss functions in Section II. System model and our proposed scheme are addressed in Section III. Furthermore, the neural network architecture and our proposed DDPM-based algorithms for probabilistic constellation shaping are addressed in this section. Numerical results are studied in Section IV. Finally, Section V concludes the paper.

Notations: Vectors and matrices are represented, respectively, by bold lower-case and upper-case symbols. $|\cdot|$ and $\|\cdot\|$ respectively denote the absolute value of a scalar variable and the ℓ_2 norm of a vector. Notation $\mathcal{N}(\mathbf{x}; \boldsymbol{\mu}, \boldsymbol{\Sigma})$ stands for the multivariate normal distribution with mean vector $\boldsymbol{\mu}$ and covariance matrix $\boldsymbol{\Sigma}$ for a random vector \mathbf{x} . Similarly, complex normal distribution with the corresponding mean vector and covariance matrix is denoted by $\mathcal{CN}(\boldsymbol{\mu}, \boldsymbol{\Sigma})$. Moreover, the expected value of a random variable (RV) is denoted by $\mathbb{E}[\cdot]$. Sets are denoted by calligraphic symbols. $\mathbf{0}$ and \mathbf{I} respectively show all-zero vector and identity matrix of the corresponding size. Moreover, $[N]$, (with N as integer) denotes the set of all integer values from 1 to N , and $\text{Unif}[N]$ (for $N > 1$) denotes discrete uniform distribution with samples between 1 to N . Also, $\delta(\cdot)$ denotes the Dirac function.

II. PRELIMINARIES

Diffusion models break down the data generation process into a series of incremental “denoising” steps, during which the model corrects itself, until ultimately generating the desired samples. A diffusion model encompasses two processes, i.e., the forward and the reverse diffusion processes. In the forward diffusion process, Gaussian kernels are applied to the data samples until they follow an isotropic Gaussian distribution, while in the reverse process, the objective is to “denoise” and generate desired samples out of noise.

Consider \mathbf{x}_0 to denote a data sample from the ground-truth probability distribution $q(\mathbf{x}_0)$. The forward diffusion process can be modeled by a conditional probability distribution $q(\mathbf{x}_t|\mathbf{x}_{t-1})$ which applies the Gaussian kernel to data samples at each time-step $t \in [T]$, with \mathbf{x}_t denoting the diffused data sample at the t -th time-step, and T denoting the total number of steps during which the diffusion process is carried out. Mathematically speaking, the forward diffusion process is expressed as

$$q(\mathbf{x}_t|\mathbf{x}_{t-1}) \sim \mathcal{N}(\mathbf{x}_t; \sqrt{1 - \beta_t}\mathbf{x}_{t-1}, \beta_t\mathbf{I}), \quad (1)$$

$$q(\mathbf{x}_{1:T}|\mathbf{x}_0) = \prod_{t=1}^T q(\mathbf{x}_t|\mathbf{x}_{t-1}), \quad (2)$$

where $0 < \beta_1 < \beta_2 < \dots < \beta_T < 1$ denotes the “variance scheduling” of the Gaussian kernel. According to (2), with $T \rightarrow \infty$, a data sample \mathbf{x}_t will asymptotically follow an isotropic Gaussian distribution with covariance matrix $\Sigma = \sigma^2\mathbf{I}$ for some $\sigma > 0$ [25]. In other words, the forward diffusion process diminishes the distinct features of data samples gradually.

In order to run the forward diffusion, the mathematical model in (1) states that at each time-step $t \in [T]$, a new sample should be drawn from a conditional Gaussian distribution with mean vector $\mu_t = \sqrt{1 - \beta_t}\mathbf{x}_{t-1}$ and covariance matrix $\Sigma_t^2 = \beta_t\mathbf{I}$. Accordingly, given the variance scheduling β_t , the forward diffusion process can be realized by sampling from a normal distribution $\epsilon_{t-1} \sim \mathcal{N}(\mathbf{0}, \mathbf{I})$ and diffusing \mathbf{x}_t as follows

$$\mathbf{x}_t = \sqrt{1 - \beta_t}\mathbf{x}_{t-1} + \sqrt{\beta_t}\epsilon_{t-1}. \quad (3)$$

Exploiting the properties of the summation of two Gaussian random variables, \mathbf{x}_t at any arbitrary time step $t \in [T]$ can be directly sampled from \mathbf{x}_0 . This is known as the reparameterization trick in the ML literature [31]. In other words, (3) can be reformulated as

$$\begin{aligned} \mathbf{x}_t &= \sqrt{\bar{\alpha}_t}\mathbf{x}_0 + \sqrt{1 - \bar{\alpha}_t}\epsilon_0, \\ q(\mathbf{x}_t|\mathbf{x}_0) &\sim \mathcal{N}(\mathbf{x}_t; \sqrt{\bar{\alpha}_t}\mathbf{x}_0, (1 - \bar{\alpha}_t)\mathbf{I}), \end{aligned} \quad (4)$$

where $\bar{\alpha}_t \triangleq \prod_{i=1}^t (1 - \alpha_i)$ and $\alpha_t \triangleq 1 - \beta_t$ [31].

So far, the forward diffusion process has been formulated. The problem now shifts to reversing the process introduced in (4). Generally speaking, the goal is to generate the desired samples from an isotropic Gaussian noise \mathbf{x}_T via sampling from $q(\mathbf{x}_{t-1}|\mathbf{x}_t)$. The challenge is that finding the conditional probability distribution $q(\mathbf{x}_{t-1}|\mathbf{x}_t)$ in an exact closed-form is cumbersome. This is because for deriving the aforementioned

conditional probability, we need the distribution of all possible data samples. Nevertheless, the reverse diffusion process can be parameterized by θ to help facilitate learning a probabilistic model $p_\theta(\mathbf{x}_{t-1}|\mathbf{x}_t)$ for realizing the reverse diffusion. Based on the above-mentioned facts, we can formulate the parametric reverse process as

$$p_\theta(\mathbf{x}_{t-1}|\mathbf{x}_t) \sim \mathcal{N}(\mathbf{x}_{t-1}; \boldsymbol{\mu}_\theta(\mathbf{x}_t, t), \boldsymbol{\Sigma}_\theta(\mathbf{x}_t, t)), \quad (6)$$

$$p_\theta(\mathbf{x}_{0:T}) = p(\mathbf{x}_T) \prod_{t=1}^T p_\theta(\mathbf{x}_{t-1}|\mathbf{x}_t). \quad (7)$$

Invoking (6), in order to learn the reverse diffusion process, one needs to learn the mean vector $\boldsymbol{\mu}_\theta(\mathbf{x}_t, t)$ and the covariance matrix $\boldsymbol{\Sigma}_\theta(\mathbf{x}_t, t)$ of the conditional probability $p_\theta(\mathbf{x}_{t-1}|\mathbf{x}_t)$. Then a neural network can be trained for this purpose, and θ corresponds to the hyperparameters of that neural network. According to [25], we emphasize that the probability distribution of the reverse process could be tractable if conditioned on \mathbf{x}_0 . Intuitively speaking, \mathbf{x}_0 can be interpreted as a “reference,” towards which we can take small steps back from noise and generate the data samples. Thus, the conditional reverse step can be denoted by $q(\mathbf{x}_{t-1}|\mathbf{x}_t, \mathbf{x}_0)$. Having the conditional probabilities of $q(\mathbf{x}_t|\mathbf{x}_0)$ and $q(\mathbf{x}_{t-1}|\mathbf{x}_0)$, one can utilize Bayes rule to derive the probability distribution of the conditional reverse step as follows

$$q(\mathbf{x}_{t-1}|\mathbf{x}_t, \mathbf{x}_0) \sim \mathcal{N}(\mathbf{x}_{t-1}; \tilde{\boldsymbol{\mu}}(\mathbf{x}_t, \mathbf{x}_0, t), \tilde{\beta}_t\mathbf{I}), \quad (8)$$

where we have

$$\tilde{\boldsymbol{\mu}}(\mathbf{x}_t, \mathbf{x}_0, t) = \frac{\sqrt{\alpha_t}(1 - \bar{\alpha}_{t-1})}{1 - \bar{\alpha}_t}\mathbf{x}_t + \frac{\sqrt{\bar{\alpha}_{t-1}}\beta_t}{1 - \bar{\alpha}_t}\mathbf{x}_0, \quad (9)$$

$$\tilde{\beta}_t = \frac{1 - \bar{\alpha}_{t-1}}{1 - \bar{\alpha}_t}\beta_t. \quad (10)$$

As can be observed from (10), there is no learnable parameter within the covariance matrix in (8). Therefore, one should learn the mean vector $\tilde{\boldsymbol{\mu}}(\mathbf{x}_t, \mathbf{x}_0, t)$. Moreover, applying the reparameterization trick [31] to (9), one can rewrite \mathbf{x}_0 as

$$\mathbf{x}_0 = \frac{1}{\sqrt{\bar{\alpha}_t}}(\mathbf{x}_t - \sqrt{1 - \bar{\alpha}_t}\epsilon_t). \quad (11)$$

Hence, (9) is further simplified as follows

$$\tilde{\boldsymbol{\mu}}(\mathbf{x}_t, \mathbf{x}_0, t) = \frac{1}{\sqrt{\alpha_t}}\left(\mathbf{x}_t - \frac{1 - \alpha_t}{\sqrt{1 - \bar{\alpha}_t}}\epsilon_t\right). \quad (12)$$

To learn the conditioned probability distribution $p_\theta(\mathbf{x}_{t-1}|\mathbf{x}_t)$ for the reverse diffusion process, it now suffices to train a neural network with the objective of approximating $\tilde{\boldsymbol{\mu}}(\mathbf{x}_t, \mathbf{x}_0, t)$. To do so, one can formulate the approximated mean vector $\boldsymbol{\mu}_\theta(\mathbf{x}_t, t)$ with the same mathematical form as the ground-truth mean vector $\tilde{\boldsymbol{\mu}}(\mathbf{x}_t, \mathbf{x}_0, t)$. Moreover, considering the fact that at time-step t , \mathbf{x}_t is known, the neural network can equivalently approximate ϵ_t . Therefore, $\boldsymbol{\mu}_\theta(\mathbf{x}_t, t)$ can be expressed as

$$\boldsymbol{\mu}_\theta(\mathbf{x}_t, t) = \frac{1}{\sqrt{\alpha_t}}\left(\mathbf{x}_t - \frac{1 - \alpha_t}{\sqrt{1 - \bar{\alpha}_t}}\epsilon_\theta(\mathbf{x}_t, t)\right), \quad (13)$$

where $\epsilon_\theta(\mathbf{x}_t, t)$ represents the output of the neural network. Now the goal is to minimize the difference between $\boldsymbol{\mu}_\theta(\mathbf{x}_t, t)$

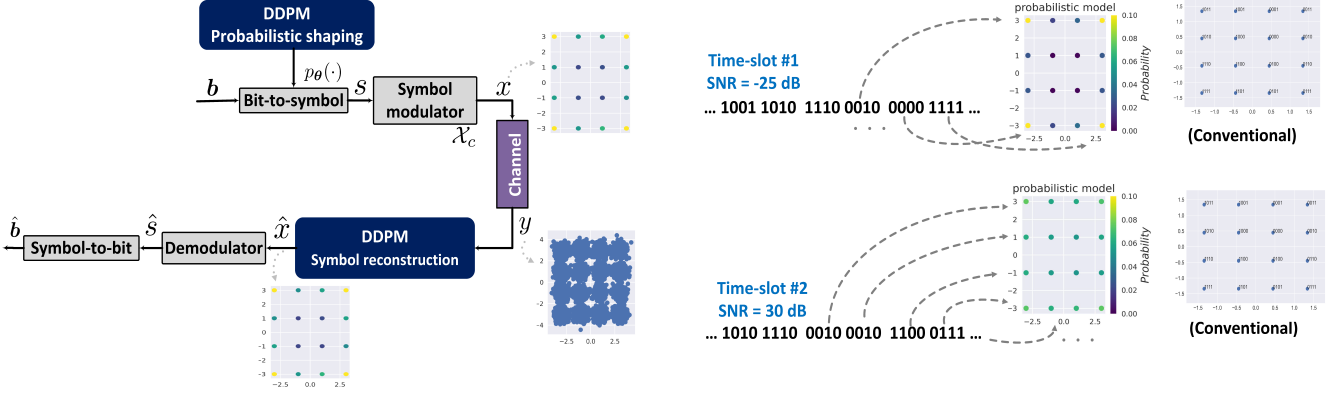


Fig. 1: System model overview. Blocks that are colored in dark blue are of interest in this work.

and $\tilde{\mu}(\mathbf{x}_t, \mathbf{x}_0, t)$. Hence, the corresponding loss function \mathcal{L}_t ($\forall t \in [T]$) for the reverse diffusion framework can be formulated as

$$\begin{aligned} \mathcal{L}_t &= \mathbb{E}_{t \sim \text{Unif}[T]} \left[\|\epsilon_t - \epsilon_\theta(\mathbf{x}_t, t)\|^2 \right] \\ &\quad \mathbf{x}_0 \sim q(\mathbf{x}_0) \\ &\quad \epsilon_0 \sim \mathcal{N}(\mathbf{0}, \mathbf{I}) \\ &= \mathbb{E}_{t \sim \text{Unif}[T]} \left[\|\epsilon_t - \epsilon_\theta(\sqrt{\bar{\alpha}_t} \mathbf{x}_0 + \sqrt{1 - \bar{\alpha}_t} \epsilon_t, t)\|^2 \right], \\ &\quad \mathbf{x}_0 \sim q(\mathbf{x}_0) \\ &\quad \epsilon_0 \sim \mathcal{N}(\mathbf{0}, \mathbf{I}) \end{aligned} \quad (14)$$

where ϵ_t denotes the diffused noise at time step t , and $\epsilon_\theta(\mathbf{x}_t, t)$ denotes the approximated noise vector at the output of the neural network. The diffusion model is trained based on the loss function given in (14), using an error measure, e.g., the widely-used MSE, between the injected and the predicted noise, where in our case, \mathbf{x}_0 stands for data samples from the constellation symbols in \mathcal{X}_c . Invoking (14), we also emphasize that $\bar{\alpha}_t, \forall t \in [T]$, is a function of the variance scheduling β_t that can help design different loss functions \mathcal{L}_t during training. This leads to the fact that different noise levels would be seen during training, which can make the system robust against a wide range of noise levels during the sampling phase as well.

III. SYSTEM MODEL AND PROPOSED SCHEME

In this section, we first present our system model. Then, our DDPM-based solution and the corresponding algorithms for probabilistic constellation shaping are proposed.

A. System Model

Fig. 1 demonstrates the communication system model considered in this paper. The system takes the information bit-stream and maps it onto hypersymbols $s \in \mathcal{S}$ according to the learnable distribution $p_\theta(s)$ (parameterized by θ), where $\mathcal{S} = \{1, \dots, M\}$ denotes the set of all hypersymbols, and M denotes the modulation order. In this paper, the probabilistic constellation shaping $p_\theta(s)$ is realized by a DDPM, which is trained and employed at the transmitter and the receiver. Details on the training and sampling processes of the employed DDPM are elaborated in the next subsection. The sequence of hypersymbols is then fed into a symbol

modulator which maps each symbol s into a constellation point $x \in \mathcal{X}_c$, with \mathcal{X}_c showing the set of constellation points. Each symbol is generated according to the distribution $p_\theta(s)$. In other words, the frequency of sending a bit-stream over the constellation point $x = g(s)$ corresponds to the parametric distribution $p_\theta(s)$, where g denotes the modulation functionality. Accordingly, the distribution of $x, \forall x \in \mathcal{X}_c$, can be written as

$$p_\theta(x) = \sum_{s \in \mathcal{S}} \delta(x - g(s)) p_\theta(s). \quad (15)$$

As explained in Section I, our focus in this paper is on probabilistic constellation shaping, and hence, the geometry of constellation is determined in advance according to network configurations.⁴ Thus, the design of modulator function $g(\cdot)$ is not of interest in this work.⁵ Accordingly, we have a one-to-one mapping between the constellation point x and the information symbol s , and one can consider that the transmitter's output is directly sampled from $p_\theta(\cdot)$. In addition, similar to [28], we assume that the bit-to-symbol mapper is known. Information-bearing signal x is then sent over the communication channel, and the channel output y is observed at the receiver. Then the receiver needs to reconstruct the transmitted symbols by approximating the posterior distribution $p(s|y)$ given the channel output. To do so, the receiver leverages the DDPM, parameterized by θ with the same architecture as that of the transmitter, and maps each received sample y to a probability distribution over the set of hypersymbols \mathcal{S} . Having this approximation, symbols can be reconstructed at the receiver's demodulator (\hat{s} in Fig. 1), and the information bits can be obtained using the typical symbol-to-bit mappers.

In the next subsection, we address our proposed scheme and provide the details on how to leverage DDPMs for the considered system model.

⁴We adhere to standard constellation schemes, such as quadrature amplitude modulation (QAM), in order to propose a system which is compliant with the real-world communication systems.

⁵Mathematically speaking, the modulator can be considered as a matrix $\mathbf{C} = [\mathbf{c}_1, \dots, \mathbf{c}_i, \dots, \mathbf{c}_{2^M}]^T \in 2^M \times 2$, with rows $\mathbf{c}_i^T \in \mathbb{R}^2, i \in [2^M]$ showing the constellation point locations. One can take the product of \mathbf{C} and a one-hot vector \mathbf{s} , with the s -th element set to one, to select a constellation point corresponding to s .

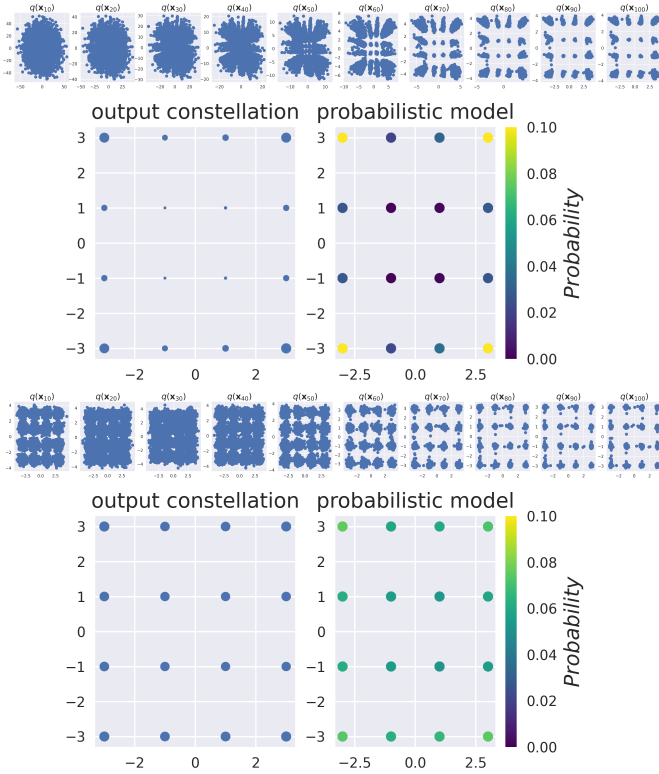


Fig. 2: A visual insight on the process of constellation shaping via our proposed scheme. From top, denoising and generation process of the diffusion model, and the probabilistic constellation shaping at the transmitter are shown, respectively. This is carried out for two different SNR values of -25 dB and 30 dB, respectively.

B. Proposed Approach

We aim to probabilistically shape the constellation symbols by finding a proper $p_{\theta}(\cdot)$, such that the information-bearing symbols sent by the transmitter, and what is inferred (reconstructed) at the receiver become as similar as possible,⁶ resulting in as few mismatches between the communication parties as possible. This fact, together with the characteristic of diffusion models to “denoise-and-generate”, motivates us to propose a DDPM-based solution for probabilistic constellation shaping. The key idea to fulfill the desired similarity is that the transmitter “mimics” the way the receiver would perform the reconstruction of symbols out of noisy signals. For instance, when the communication channel is experiencing high levels of noise, i.e., in low-SNR regime, we intuitively expect that most often, the receiver would be able to decode the symbols corresponding to the points that are relatively far from each other in the constellation geometry, while the other points are prone to being decoded incorrectly. Thus, the transmitter could assign the information bits to those constellation points that are at the furthest distance from each other, with higher probabilities. This also helps facilitate having “mutual understanding” of how to map and de-map the information symbols over time, realizing *native intelligence*

⁶This “similarity” will be quantitatively evaluated in the next section, using two widely-adopted metrics of mutual information and cosine similarity.

Algorithm 1 Training algorithm of DDPM [25]

Hyper-parameters: Number of time-steps T , neural architecture $\epsilon_{\theta}(\cdot, t)$, variance schedule β_t , and $\bar{\alpha}_t, \forall t \in [T]$.

Input: Sample points from the constellation geometry \mathcal{X}_c .

Output: Trained neural model for DDPM.

- 1: **while** the stopping criteria are not met **do**
 - 2: Randomly sample \mathbf{x}_0 from \mathcal{X}_c
 - 3: Randomly sample t from $\text{Unif}[T]$
 - 4: Randomly sample ϵ from $\mathcal{N}(\mathbf{0}, \mathbf{I})$
 - 5: Take gradient descent step on
 - 6:
$$\nabla_{\theta} \left\| \epsilon - \epsilon_{\theta}(\sqrt{\bar{\alpha}_t} \mathbf{x}_0 + \sqrt{1 - \bar{\alpha}_t} \epsilon, t) \right\|^2$$
 - 7: **end while**
-

among communication parties. To gain a visual insight on the process of constellation shaping via our proposed scheme, Fig. 2 demonstrates the shaped constellation points and their corresponding probability distribution for 16-QAM geometry for two different SNR values of -25 dB and 30 dB. More details are elaborated on in Section IV.

Motivated by the abovementioned discussions, our step-by-step solution can be elaborated on as follows.

1) *DDPM Training:* A DDPM is trained based on the loss function given in (14). This corresponds to training the parameter θ for our probabilistic shaping scheme in (15). The process is summarized in Algorithm 1. We take a random sample \mathbf{x}_0 from the set of constellation points \mathcal{X}_c ; We also sample a random time-step $t \sim \text{Unif}[T]$. A noise vector ϵ (with the same shape as the input) is also sampled from the normal distribution. Given the sampled time-step t , the noise level is adjusted according to the variance scheduling β_t . We then make the input vector \mathbf{x}_0 noisy according to (4). The neural network is trained based on (14) to approximate the noise vector lying in the noisy data. Training can be carried out in a central cloud, or an edge server, and then, the trained model is downloaded by the communication entities. Note that the same trained model is deployed at both the transmitter and the receiver, and they use it to run their DDPM-based framework for the constellation generation and decoding, respectively.

2) *Link quality estimation with channel SNR:* Within each transmission slot, the transmitter first estimates the quality of the communication link. This is done using the pilot signal sent by the destination node at the beginning of each transmission slot, and the SNR level of communication channel can be calculated [34].

3) *Probabilistic shaping at the transmitter:* The DDPM is run at the transmitter to probabilistically shape (generate) the constellation symbols according to the channel SNR. To fulfill the desired “similarity” between the transmitter and the receiver, the transmitter synthetically generates samples of the received signal (with the SNR level according to the estimated channel SNR), and then tries to denoise them to infer which constellation points are more probable to be reconstructed, sending the information bits over those points. To do so, we first take N_s samples from the set of constellation symbols \mathcal{X}_c uniformly at random. The sample size N_s can be regarded as

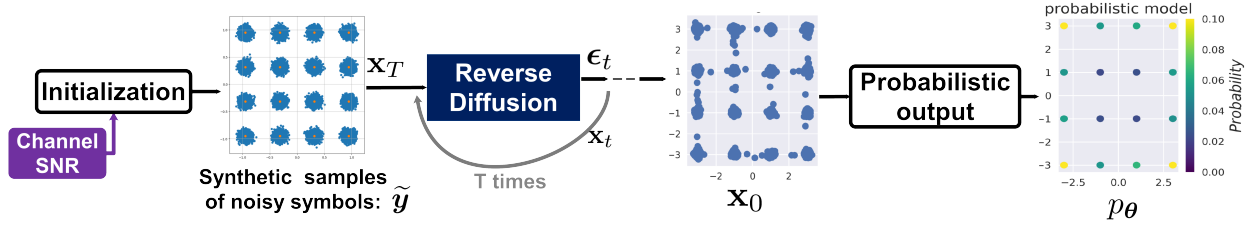


Fig. 3: Block-diagram of Algorithm 2 for the proposed scheme.

Algorithm 2 DDPM sampling: Probabilistic shaping at transmitter

Hyper-parameters: Number of time-steps T , trained neural model θ , constellation geometry \mathcal{X}_c

Input: Channel SNR Γ .

Initialization: Synthetic samples of noisy symbols:

- 1: Randomly sample $\tilde{\mathbf{x}}_s$, with size N_s , from set \mathcal{X}_c
- 2: Randomly sample $\tilde{\mathbf{n}}$, with size N_s , from $\mathcal{N}(\mathbf{0}, \mathbf{I})$
- 3: $\tilde{\mathbf{y}} = \tilde{\mathbf{x}}_s + \delta \tilde{\mathbf{n}}$

Reverse diffusion:

- 4: $\mathbf{x}_T = \tilde{\mathbf{y}}$
- 5: **for** $t = T, \dots, 1$ **do**
- 6: $\mathbf{z} \sim \mathcal{N}(\mathbf{0}, \mathbf{I})$ if $t > 1$, else $\mathbf{z} = \mathbf{0}$
- 7: $\mathbf{x}_{t-1} = \frac{1}{\sqrt{\alpha_t}} \left(\mathbf{x}_t - \frac{1-\alpha_t}{\sqrt{1-\alpha_t}} \epsilon_\theta(\mathbf{x}_t, t) \right) + \sqrt{1-\alpha_t} \mathbf{z}$
- 8: **end for**

Probabilistic output:

- 9: $\psi = \text{proj}_{\mathcal{X}_c}(\mathbf{x}_0)$
 - 10: $\mathbf{c} = \text{count}(\psi, \mathcal{X}_c)$
 - 11: **return** $p_\theta = \mathbf{c}/N_s$
-

the number of observations to form (generate) the empirical distribution of our probabilistic shaping. In addition, we sample N_s realizations of random noise with average power δ^2 , and inject them into the uniformly-sampled symbols. The power of synthetic noise, δ^2 , is calculated according to the channel SNR, Γ , which was obtained at Step 2. This can be formulated as

$$\delta^2 = 10^{\Gamma/10} P, \quad (16)$$

where P denotes the average transmit power. The noisy version of samples is then fed into the trained DDPM, and the reverse diffusion process is run to denoise and generate symbols out of the synthetically-noisy samples. The distribution of the generated samples at the output of the DDPM block is considered as the output probabilistic constellations, onto which the information symbols are mapped to be sent.

The overall algorithm is proposed in Algorithm 2. Moreover, a block-diagram of the proposed probabilistic constellation shaping algorithm is illustrated in Fig. 3. In Algorithm 2, Lines 2 to 3 correspond to the synthetic generation of noisy received signals, given the channel SNR. Moreover, the main loop corresponds to the reverse diffusion process from time-step T to 1, according to 13, which tries to mimic the denoising functionality of the receiver, using the trained DDPM. Also, $\text{proj}_{\mathcal{S}}(\mathbf{x})$ stands for the projection

operator, which maps the elements of vector \mathbf{x} onto the nearest elements in the set \mathcal{S} . Moreover, $\text{count}(\mathbf{x}, \mathcal{S})$ outputs a vector with size $|\mathcal{S}|$, with elements representing the number of occurrences of the elements of set \mathcal{S} in vector \mathbf{x} . Notably, ψ in Algorithm 2 denotes the probabilistically-shaped constellation points at the output of the transmitter's DDPM block, and p_θ stands for the corresponding distribution inferred by the diffusion model. In the next section, data visualization of different steps are presented with numerical examples, to further understand what is going on in the proposed constellation shaping algorithm.

4) *Symbol reconstruction at the receiver:* After generating constellation symbols, information signals are transmitted according to the probabilistic model of the constellation points. The symbols are then received by the receiver, and it runs the diffusion model to reconstruct (regenerate) the symbols from the noisy received signals. The corresponding algorithm for this step is proposed in Algorithm 3. Starting from the received batch of noisy symbols, denoted by \mathbf{y} , for each time step $t \in \{T, T-1, \dots, 1\}$, the neural network outputs $\epsilon_\theta(\hat{\mathbf{x}}_t, t)$ to approximate the residual noise within the batch of symbols, and the sampling algorithm is run according to Line 4 of the algorithm, in order to sample $\hat{\mathbf{x}}_{t-1}$. The process is executed for T steps.⁷

To summarize Section III-B, a general overview of the proposed scheme is illustrated in Fig. 4.

IV. NUMERICAL EXPERIMENTS

In this section, we carry out different numerical evaluations in terms of mutual information metric and cosine similarity, in order to highlight the performance of the proposed scheme compared to other benchmarks. We show that our DDPM-based approach achieves 30% improvement in terms of cosine similarity, and a threefold improvement in terms of mutual information metric compared to DNN-based approach. We also show that our proposed scheme maintains *native resilience* as well as *robust out-of-distribution performance* under low-SNR regime and non-Gaussian assumptions.

To parameterize the reverse diffusion process of our DDPM-based scheme, we employ a neural network comprised of 3 hidden conditional layers (with softplus activation functions), each with 128 neurons conditioned on t . The output layer is a linear layer with the same size as the input.

⁷We emphasize that within each transmission slot, while the channel coherence time is respected, the channel SNR remains unchanged compared to the one that is utilized by the transmitter for the constellation shaping.

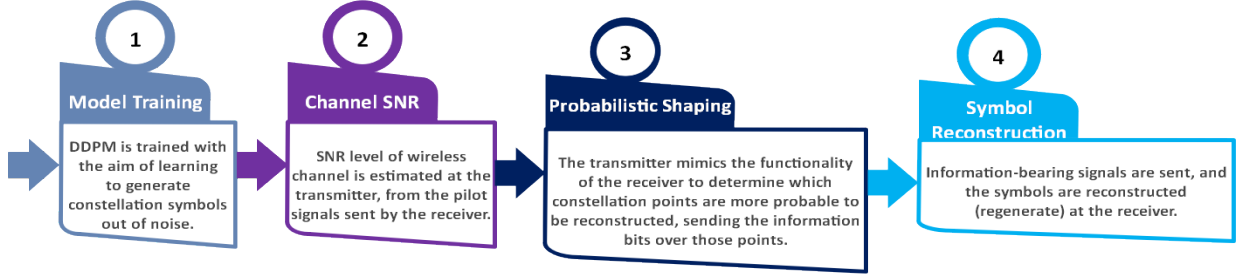


Fig. 4: Summary of the proposed approach.

Algorithm 3 DDPM sampling: Symbol reconstruction at receiver

Hyper-parameters: Number of time-steps T , trained neural model θ , constellation geometry \mathcal{X}_c

Input: Received signal \mathbf{y}

- 1: $\hat{\mathbf{x}}_T = \mathbf{y}$
 - 2: **for** $t = T, \dots, 1$ **do**
 - 3: $\mathbf{z} \sim \mathcal{N}(\mathbf{0}, \mathbf{I})$ if $t > 1$, else $\mathbf{z} = \mathbf{0}$
 - 4: $\hat{\mathbf{x}}_{t-1} = \frac{1}{\sqrt{\alpha_t}} \left(\hat{\mathbf{x}}_t - \frac{1-\alpha_t}{\sqrt{1-\alpha_t}} \epsilon_{\theta}(\hat{\mathbf{x}}_t, t) \right) + \sqrt{1-\alpha_t} \mathbf{z}$
 - 5: **end for**
 - 6: **return** $\text{proj}_{\mathcal{X}_c}(\hat{\mathbf{x}}_0)$
-

Instead of training T distinct models for each time-step, we employ only one neural model for the entire denoising time-steps. This is done via sharing the parameters of the neural network across time-steps—we encode the time-steps $t \in [T]$ and input it to each hidden layer of our neural network as a vector embedding, as illustrated in Fig. 5. The hidden layers are conditioned on t via being multiplied by the time embeddings [5], [22], [25]. Intuitively speaking, incorporating the time-step into the neural network makes our model “know” at which particular time-step it is operating for every sample. To stabilize the training algorithm of our DDPM framework, exponential moving average (EMA) method is implemented [36]. To elaborate, instead of directly updating the weights, a copy of the previous weights is kept, and the weighted average between the previous and new version of the weights are calculated for the model update. This helps maintain model momentum. For the diffusion process, the variance scheduling, α_t is set to constants decreasing from $\alpha_1 = 0.99999$ to $\alpha_T = 0.99$ with Sigmoid scheduling [37]. For training the diffusion model, we use adaptive moment estimation (Adam) optimizer with learning rate $\lambda = 10^{-3}$. We consider QAM geometry as a widely-adopted constellation format in wireless networks [7], [9], [28]. Moreover, we set $T = 100$ and $T = 200$ for 16-QAM and 64-QAM geometry, respectively. The stopping criterion in Algorithm 1 is met when reaching the maximum number of epochs [21], [22], which is set to 1000 epochs for 16-QAM and 5000 epochs for 64-QAM. The training process for the case of 16-QAM geometry is illustrated in Fig. 6. We can observe a decreasing trend in the training loss function over epochs. The same trend could be observed for 64-QAM case, and we do not repeat

the figure due to space limitations.

A. Data Visualization of The Proposed Approach

In this subsection, we carry out data visualization for the generation process of our DDPM-based solution during training and sampling.

Figs. 7 and 8 visualize the reverse diffusion process across epochs during the training of the implemented DDPM. For these figures, we take “snapshots” of the model (i.e., we save the model’s current state) at specific checkpoints (epochs) during the training process, and plot the output of the DDPM block over time-steps. As can be seen from the figures, the employed DDPM gradually learns to generate the desired samples (constellation symbols) out of an isotropic Gaussian noise. Moreover, we can observe from the figures that as we reach the maximum number of epochs, the model can sooner (i.e., in fewer time-steps) generate the data samples.

In Fig. 9, we carry out data visualization for sampling phase over different SNR values. Data visualizations demonstrated in this figure correspond to Algorithms 2 and 3. The first row corresponds to data visualization of the reverse diffusion process for generating constellation points, the second row corresponds to the probabilistic constellation shaping steps that are performed at the transmitter (Algorithm 2), and the third row corresponds to the reconstruction at the receiver (Algorithm 3). This is repeated for different SNRs. According to data visualizations for the reverse diffusion process, our results show that even when the power of noise is more than 300 times of the signal ($\Gamma = -25$) we can have a clear understanding of the underlying constellation scheme at the end of running the diffusion model. Also, having higher SNRs results in more clear generation and reconstruction of constellation samples. To explain the second and the third rows of Fig. 9 for each SNR value, we can provide the following discussions. For each SNR level, we start with $N_s = 10000$ uniformly-sampled constellation points (the first sub-figure), synthetically add Gaussian noise to the samples, and run the DDPM according to Algorithm 2. We then map the generated samples (the third sub-figure) to the nearest constellation point in set \mathcal{X}_c which results in the fourth sub-figure, in which the size of the points is proportional to their probabilities of occurrence. Finally, by counting the number of occurrence (generation) of each constellation symbol generated at the output of the DDPM block, the probabilistic

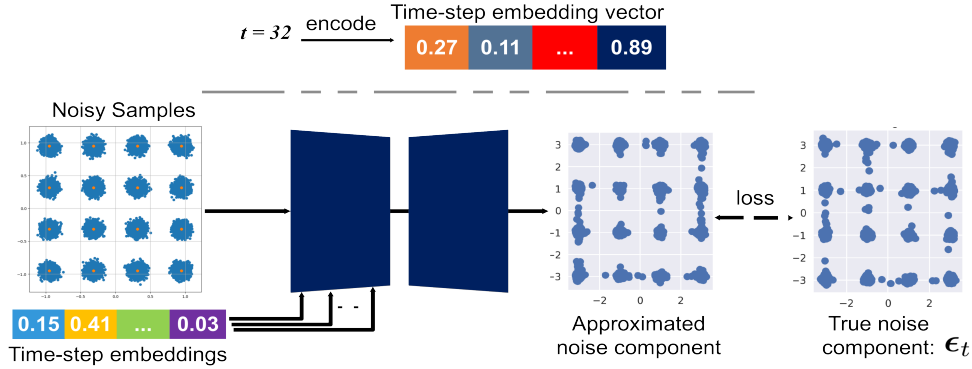


Fig. 5: Block diagram of training the diffusion model. Time-steps are incorporated into the hidden layers as embedding vectors.

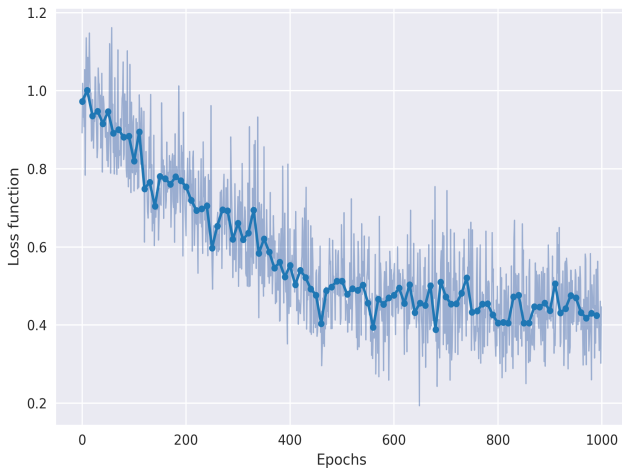


Fig. 6: Training process of DDPM over epochs.

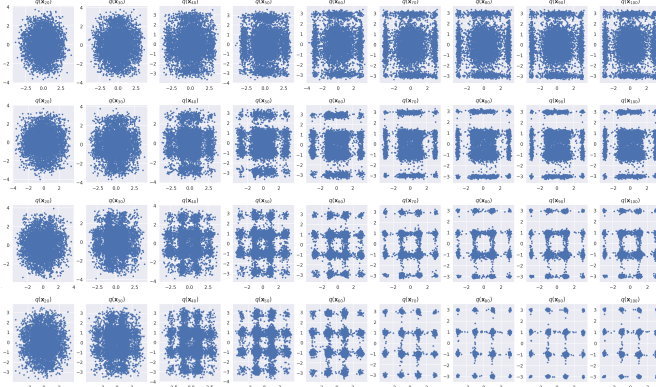


Fig. 7: Data visualization for the reverse diffusion process during training (16-QAM). From top to bottom, the rows correspond to epochs 200, 300, 400, and 1000, respectively.

model of the constellation points is obtained (the fifth sub-figure). Afterward, information symbols can be mapped onto the constellation points based on the distribution obtained from the probabilistic model. The probabilistically-shaped information symbols are passed through the communication channel and received by the receiver end as denoted by \mathbf{y} . The

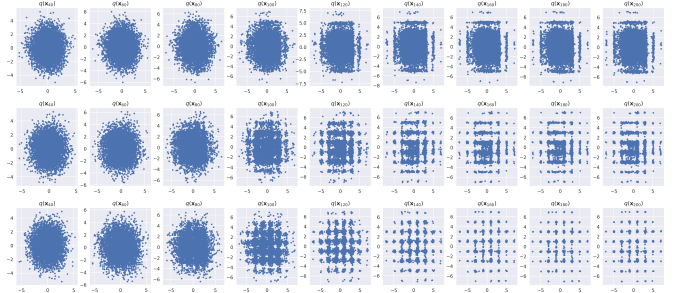


Fig. 8: Data visualization for the reverse diffusion process during training (64-QAM). From top to bottom, the rows correspond to epochs 1500, 2500, and 4500, respectively.

receiver then runs the DDPM model based on Algorithm 3, reconstructs, and decodes the constellation symbols, as shown in the third row of Fig. 9 for each SNR level. Comparing the output of our probabilistic constellation generation algorithm (the second row) and the reconstructed symbols at the receiver (the third row), we can observe that the idea of mimicking the functionality of receiver for shaping the constellation symbols (addressed in Section III-B) has helped the transmitter generate symbols that are quite similar to the ones that are actually reconstructed by the receiver. This improves the communication performance by significantly decreasing the mismatch between the way the transmitter conveys the information, and the way the receiver decodes the symbols. This “similarity” is quantitatively measured in terms of mutual information and cosine similarity in the subsequent figures.

To further study the behaviour of our proposed scheme over different SNR values, we can provide the following explanations. According to the results of Fig. 9, when the communication system is experiencing low-SNR regimes (e.g., -25 dB or -10 dB in the figure), the probabilistic model at the output of transmitter’s DDPM demonstrates a non-uniform distribution over constellation points, with higher probabilities assigned to the points that are at the furthest distance from each other in the constellation geometry. This is aligned with what we intuitively expect from a communication system under low-SNR regimes to frequently map information bits

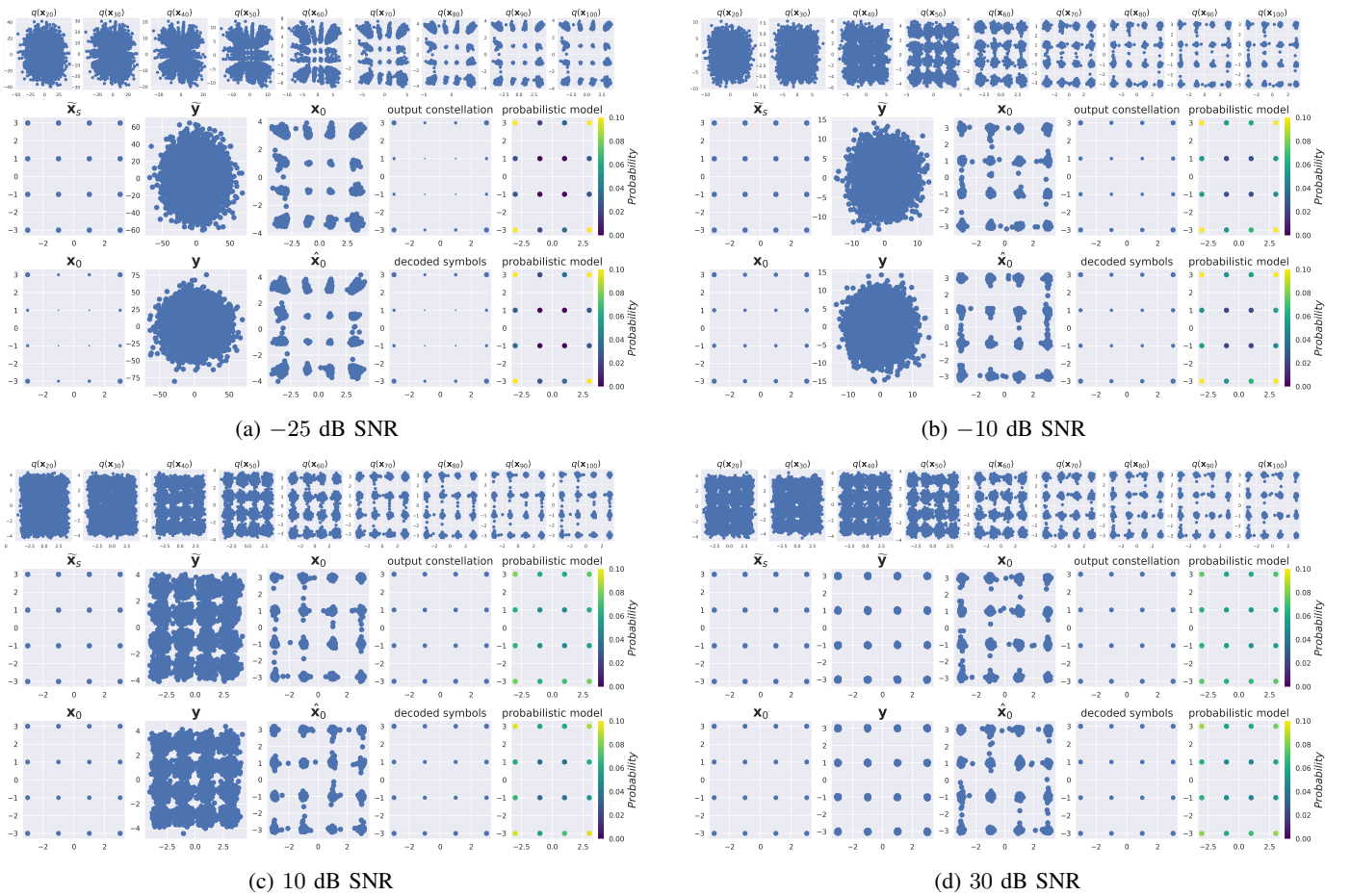


Fig. 9: Probabilistic constellation shaping process at the transmitter, and the symbol reconstruction at the receiver. From top to bottom, the first row visualizes the reverse diffusion process during sampling phase, the second row corresponds to the probabilistic constellation shaping algorithm, and the third row corresponds to the reconstruction at the receiver.

to constellation symbols that are far apart from each other, in order to decrease the decoding error. Increasing the SNR, we can see from the figure that the probabilistic shaping tends to uniform distribution, which is also aligned with one’s intuition about communication systems. We finally mention that our results for 64-QAM scenario also demonstrated quite the same results where we do not repeatedly mention them here for the sake of brevity.

B. Performance Evaluation and Resilience

In this subsection, we present quantitative evaluations of our proposed scheme and show its *resilience* against low-SNR regimes, as well as *out-of-distribution (OOD) robustness* for non-Gaussian noise. We also compare our results with different benchmarks.

Fig. 10 demonstrates the mutual information between the generated symbols at the output of transmitter’s DDPM (i.e., the channel input), and the reconstructed ones at the receiver. The mutual information metric can be considered as a fundamental measure to quantitatively assess the “mutual similarity” between the communication nodes. For this experiment, we consider both cases of additive white Gaussian noise (AWGN) channel and also non-Gaussian noise

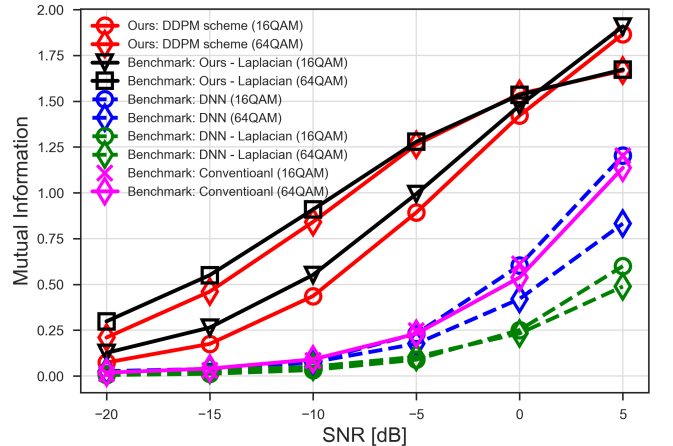


Fig. 10: Mutual information between the generated symbols at transmitter and the reconstructed ones at the receiver for AWGN channel and non-Gaussian noise.

to highlight the OOD performance of our scheme. For the DNN benchmark, we consider a learning-based scenario with

trainable constellation layer and neural demapper [28].⁸ The DNN benchmark has three linear layers with 64 neurons and rectified linear unit (ReLU) activation functions [33]. We note that based on our ablation studies, increasing the depth of the DNN, or the number of hidden neurons does not result in a significant improvement in its performance. For both 16- and 64-QAM benchmarks, we considered 5000 training iterations with Adam optimizer [33]. Considering the general behaviour of mutual information versus SNR in this figure, we can observe that by increasing the SNR level, it becomes more straightforward for both the transmitter and the receiver to denoise and generate the symbols, which is also aligned with one’s intuition. Hence, the mutual information increases with the SNR as can be observed from the figure. The increasing trend of mutual information vs. SNR also applies to the DNN benchmark, since a typical DNN can also perform the inference with higher accuracy when given less noisy input.

Fig. 10 highlights the performance of our proposed DDPM-based scheme compared to the DNN-based approach and the conventional uniform shaping. While the conventional and DNN benchmarks do not exhibit any significant performance in SNR ranges below -5 dB, our scheme achieves a mutual information of around 1 bit for 16-QAM case, and 1.25 bits for 64-QAM case, respectively. In addition, one can observe a threefold improvement in terms of mutual information between the communication sides compared to DNN-based benchmark at 0 dB SNR. These results clearly highlight that our main goal in realizing the “mutual understanding” among communication parties has been successfully achieved, and thanks to this understanding, the system is resilient under low-SNRs. To show the robustness of our scheme for OOD performance, we study the scenario of communication channels with non-Gaussian noise [9]. Specifically, for this experiment we consider additive Laplacian noise with the same variance as that of AWGN scenario. Remarkably, although we do not re-train our diffusion model with Laplacian noise, the performance of our DDPM-based approach does not change under this OOD scenario, and the resultant mutual information curves follow the case of in-distribution scenario. However, we can see from the figure that the DNN benchmark experiences performance degradation under non-Gaussian assumption, although we also re-trained it with Laplacian noise. For example, for 16-QAM geometry and 5 dB SNR, the mutual information of DNN benchmark decreases by more than 50% in Laplacian case.

In Fig. 11, we further study the performance of our proposed scheme in terms of cosine similarity, over a wide range of SNR values from -30 dB to 30 dB. The cosine similarity is a widely-adopted measure in data science to quantify the similarity between two vectors, \mathbf{x}_0 and $\hat{\mathbf{x}}_0$ [38]. It can be formulated as

$$\text{CSIM} = \frac{\mathbf{x}_0^T \hat{\mathbf{x}}_0}{\|\mathbf{x}_0\| \|\hat{\mathbf{x}}_0\|}. \quad (17)$$

⁸Generally speaking, this benchmark is already implemented by Sionna (an open source library developed and used by NVIDIA to carry out 6G research), which is referred to trainable constellation, and it is considered as one of the key advantages of Sionna for ML-based research [33].

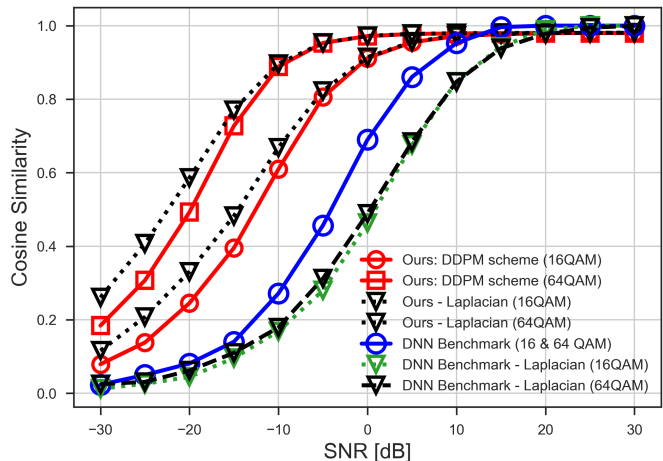
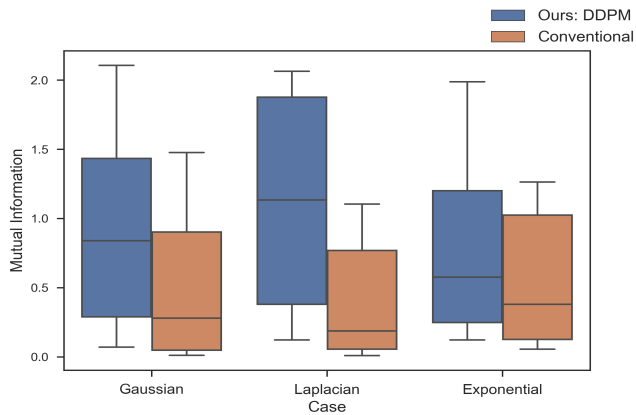


Fig. 11: Cosine similarity between transmitter’s generated symbols and the reconstructed ones at the receiver.

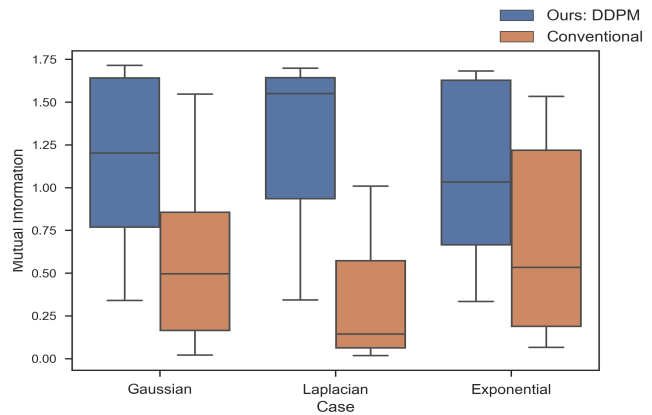
Here, we calculate the cosine similarity between the output constellation symbols at the transmitter, and the reconstructed ones at the receiver. Since we have 2-D constellation points as I/Q samples, we take the cosine similarity of I and Q samples separately, and then normalized it to 1. Notably, the figure highlights that our proposed approach leads to competitive in- and out-of-distribution performance when compared to DNN-based benchmarks. For example, for -5 dB SNR and 64-QAM geometry, the system maintains the “mutual similarity” between the communication parties such that more than 50% improvement could be observed in terms of cosine similarity compared to the DNN benchmark. Moreover, while the performance of DNN benchmark degrades when having non-Gaussian noise, our scheme achieves the same (or even better) results and maintains its robustness.

We now consider a different setup, in order to take into account the variations of wireless channel (equivalently the channel SNR in our system model), over the transmission time-slots. This is different from the previous simulation setups, for which we set a fixed SNR value, simulated the communication system, and derived the performance metrics for each SNR. To this end, we run the probabilistic shaping algorithm multiple times, each time considering a different channel SNR which is chosen randomly from the set of SNR levels $\{-20, -19, \dots, 9, 10\}$. Now we are interested in the distribution of our performance metrics derived over those realizations.

Figs. 12 and 13 demonstrate, respectively, the distribution of mutual information, and the cosine similarity achieved over 30 realizations of our diffusion-based probabilistic constellation shaping (each with empirical sample size of $N_s = 10000$), versus the conventional (non-learning) uniform shaping. The distributions are illustrated as box-plots so that we can graphically show the locality and skewness, as well as the variation in the performance metrics derived over time. The results are obtained for three different scenarios, i.e., the in-distributions scenario with Gaussian noise, and the OOD scenario with Laplacian and exponential noise [9], without

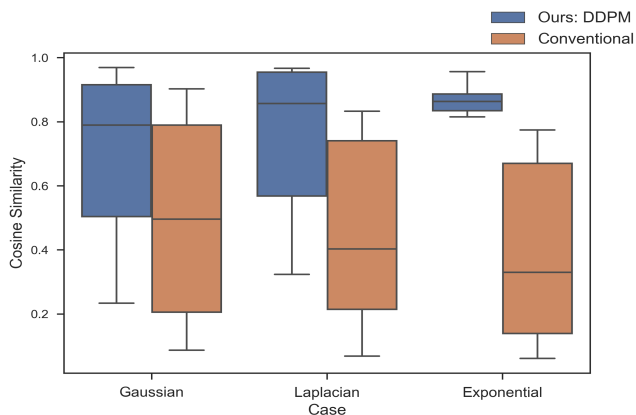


(a) 16-QAM

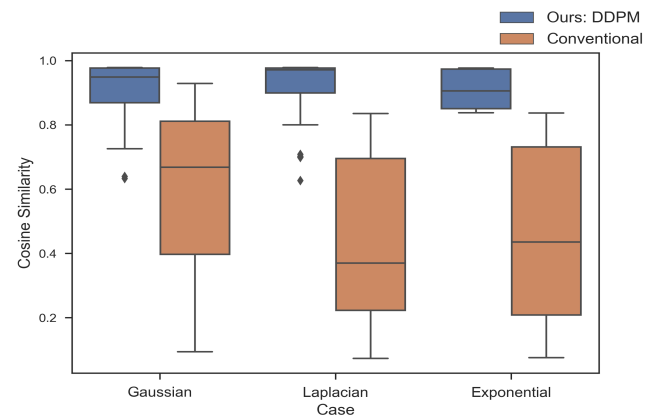


(b) 64-QAM

Fig. 12: Performance of our proposed scheme in terms of mutual information for both in- and out-of-distribution scenarios.



(a) 16-QAM



(b) 64-QAM

Fig. 13: Performance of our proposed scheme in terms of cosine similarity for both in- and out-of-distribution scenarios.

re-training the model. We can infer from the figures that our proposed scheme significantly outperforms the conventional uniform shaping in different scenarios, as for most of the plots, the median line of the performance metrics for our scheme lies outside the box of the corresponding conventional baseline. Furthermore, our proposed scheme consistently outperforms the conventional scheme, achieving higher median and maximum performance metrics in all of the scenarios. We can also see from the figures that the generative AI-based approach even performs better with the increase in the modulation order (which is also aligned with the per-SNR results in Figs. 10 and 10), while the conventional approach experiences performance degradation in 64-QAM case. Considering the OOD scenario with Laplacian noise, the figures imply that the performance of the conventional baseline decreases over time, in both 16-QAM and 64-QAM cases. This is due to the fact that the conventional solutions are optimized with the underlying assumption of Gaussian distribution, and they typically lead to non-optimal solutions for other types of noise [9]. On the other hand, our DDPM-based approach does not show any performance degradation in terms of mutual information, nor in terms of cosine

similarity. We finally mention that for the special case of exponential noise, the conventional baseline might perform better than the Laplacian scenario. This is due to the fact that with exponential noise, the system observes a one-sided distribution for the additive noise, and hence, it would be easier to decode the symbols than the case of Laplacian noise.

V. CONCLUSIONS

In this paper, we have proposed DDPM-based probabilistic constellation shaping for wireless communications. exploiting the “denoise-and-generate” characteristic of diffusion models, we have offered a radically different approach for PHY design based on generative AI. The key idea was that the transmitter mimics the way the receiver would do to reconstruct (regenerate) the symbols out of noisy signals, realizing “reciprocal understanding” to reduce the mismatches among communication parties. Our results have highlighted the performance of our scheme compared to other benchmarks, while providing *network resilience* under low-SNR regimes and non-Gaussian noise. We have achieved 30% improvement in terms of cosine similarity and a threefold improvement in terms of mutual information compared to DNN-based approach for 64-QAM

geometry. We believe that our results in this paper can pave the way towards a new paradigm of generative AI-based signal design for the future generations of communication systems.

REFERENCES

- [1] M. Letafati, S. Ali, and M. Latva-aho, "Probabilistic constellation shaping with denoising diffusion probabilistic models: A novel approach," *arXiv preprint arXiv:2309.08688*, Sep. 2023.
- [2] P. Popovski. (2023, Jun. 11). "Communication engineering in the era of generative AI." *Medium*, [Online]. Available: <https://petarpopovski-51271.medium.com/communication-engineering-in-the-era-of-generative-ai-703f44211933>
- [3] M. Letafati, S. Ali, and M. Latva-aho, "WiGenAI: The symphony of wireless and generative AI via diffusion models," *arXiv preprint arXiv:2310.07312*, Oct. 2023.
- [4] "What is Generative AI?," *NVIDIA*, [Online]. Available: <https://www.nvidia.com/en-us/glossary/data-science/generative-ai/>, [Accessed Aug. 24, 2023].
- [5] L. Yang, *et al.*, "Diffusion models: A comprehensive survey of methods and applications," *ACM Computing Surveys*, Sep. 2023.
- [6] 3GPP Release 18, "Study on Artificial Intelligence (AI)/Machine Learning (ML) for NR Air Interface RAN," Meeting #112, Athens, Greece, Tech. Rep., 27th February – 3rd March 2023.
- [7]
- [8] S. Ali, *et al.*, "6G white paper on machine learning in wireless communication networks," *arXiv preprint arXiv:2004.13875*, Apr. 2020.
- [9] M. Chafii, L. Bariah, S. Muhaidat, and M. Debbah, "Twelve scientific challenges for 6G: Rethinking the foundations of communications theory," *IEEE Communications Surveys & Tutorials*, vol. 25, no. 2, pp. 868–904, Second quarter 2023.
- [10] F. A. Aoudia, J. Hoydis, A. Valcarce, and H. Viswanathan, "Toward a 6G AI-native air interface," *Nokia Bell Labs*, Mar. 2021. [Online]. Available: <https://onestore.nokia.com/asset/210299>.
- [11] M. Honkala, D. Korpi, and J. M. J. Huttunen, "DeepRx: Fully convolutional deep learning receiver," *IEEE Transactions on Wireless Communications*, vol. 20, no. 6, pp. 3925–3940, Jun. 2021.
- [12] F. A. Aoudia and J. Hoydis, "Model-free training of end-to-end communication systems," *IEEE Journal on Selected Areas in Communications*, vol. 37, no. 11, pp. 2503–2516, Nov. 2019.
- [13] J. M. J. Huttunen, D. Korpi, and M. Honkala, "DeepTx: Deep learning beamforming with channel prediction," *IEEE Transactions on Wireless Communications*, vol. 22, no. 3, pp. 1855–1867, Mar. 2023.
- [14] D. Korpi, M. Honkala, J. M. J. Huttunen, F. A. Aoudia, and J. Hoydis, "Waveform learning for reduced out-of-band emissions under a nonlinear power amplifier," *arXiv preprint arXiv: 2201.05524*, Jan. 2022.
- [15] S. F. Yilmaz, X. Niu, B. Bai, W. Han, L. Deng, and D. Gündüz "High perceptual quality wireless image delivery with denoising diffusion models," *arXiv preprint arXiv:2309.15889v1*, Sep. 2023.
- [16] J. Chen, D. You, D. Gündüz, and P. L. Dragotti "CommIN: Semantic image communications as an inverse problem with INN-guided diffusion models," *arXiv preprint arXiv:2310.01130*, Oct. 2023.
- [17] T. Wu, Z. Chen, D. He, L. Qian, Y. Xu, M. Tao, W. Zhang, "CDDM: Channel denoising diffusion models for wireless communications," *arXiv preprint arXiv: 2305.09161*, May 2023.
- [18] M. Arvinte and J. I. Tamir, "Score-based generative models for robust channel estimation," *2022 IEEE Wireless Communications and Networking Conference (WCNC)*, Austin, TX, USA, 2022, pp. 453–458.
- [19] M. Letafati, S. Ali, and M. Latva-aho, "Denoising diffusion probabilistic models for hardware-impaired communications," *arXiv preprint arXiv:2309.08568*, Oct. 2023.
- [20] S. Gong, M. Li, J. Feng, Z. Wu, and L. Kong, "DiffuSeq: Sequence to sequence text generation with diffusion models," *arXiv preprint arXiv:2210.08933*, Feb. 2023.
- [21] A. Blattmann, R. Rombach, H. Ling, T. Dockhorn, S. W. Kim, S. Fidler, and K. Kreis, "Align your latents: High-resolution video synthesis with latent diffusion models," in *Proceedings of the IEEE/CVF Conference on Computer Vision and Pattern Recognition (2023)*, pp. 22563–22575.
- [22] Q. Yan, Z. Liang, Y. Song, R. Liao, and L. Wang, "SwinGNN: Rethinking permutation invariance in diffusion models for graph generation," *arXiv preprint arXiv:2307.01646*, Jul. 2023.
- [23] B. Levac, A. Jalal, K. Ramchandran, and J. I. Tamir, "MRI reconstruction with side information using diffusion models," *arXiv:2303.14795*, Jun. 2023. [Online]. Available: <https://arxiv.org/abs/2303.14795>.
- [24] G. Lin, A. Milan, C. Shen, and I. Reid, "RefineNet: Multi-path refinement networks for high-resolution semantic segmentation," in *Proc. IEEE Conf. Comput. Vis. Pattern Recognit. (CVPR)*, Jul. 2017, pp. 1925–1934.
- [25] J. Ho, A. Jain, and P. Abbeel, "Denoising diffusion probabilistic models," *Advances in Neural Information Processing Systems*, vol. 33, pp. 6840–6851, 2020.
- [26] F. A. Aoudia and J. Hoydis, "Waveform learning for next-generation wireless communication systems," *IEEE Transactions on Communications*, vol. 70, no. 6, pp. 3804–3817, Jun. 2022.
- [27] F. A. Aoudia and J. Hoydis, "End-to-end waveform learning through joint optimization of pulse and constellation shaping," *2021 IEEE Globecom Workshops (GC Wkshps)*, Madrid, Spain, Dec. 2021, pp. 1–6.
- [28] M. Stark, F. A. Aoudia, and J. Hoydis, "Joint learning of geometric and probabilistic constellation shaping," *2019 IEEE Globecom Workshops (GC Wkshps)*, Waikoloa, HI, USA, 2019, pp. 1–6.
- [29] [Release 16] 3GPP, "Physical channels and modulation." TS 38.211 (V16.2.0), July 2020.
- [30] J. Sohl-Dickstein, E. Weiss, N. Maheswaranathan, and S. Ganguli, "Deep unsupervised learning using nonequilibrium thermodynamics," *Proceedings of the 32nd International Conference on Machine Learning*, Francis R. Bach and David M. Blei (Eds.), Lille, France, Jul. 2015, vol. 37, pp. 2256–2265.
- [31] D. P. Kingma, T. Salimans, and M. Welling "Variational dropout and the local reparameterization trick," *Advances in Neural Information Processing Systems (NIPS 2015)*, vol. 28, 2015.
- [32] C. Luo, "Understanding diffusion models: A unified perspective," *arXiv preprint arXiv:2208.11970*, Aug. 2022.
- [33] J. Hoydis, S. Cammerer, F. A. Aoudia, A. Vem, N. Binder, G. Marcus, and A. Keller, "Sionna: An open-source library for next-generation physical layer research," *arXiv preprint arXiv:2203.11854*, Mar. 2023.
- [34] X. Chen, D. W. K. Ng, W. Yu, E. G. Larsson, N. Al-Dhahir, and R. Schober, "Massive access for 5G and beyond," *IEEE J. Sel. Areas Commun.*, vol. 39, no. 3, pp. 615–637, Mar. 2021.
- [35] A. Vaswani, *et al.*, "Attention is all you need," *arXiv:1706.03762v7*, Aug. 2023. [Online]. Available: <https://arxiv.org/abs/1706.03762>.
- [36] Y. Song and S. Ermon, "Improved techniques for training score-based generative models," *Advances in Neural Information Processing Systems 33 (NeurIPS 2020)*, Dec. 2020.
- [37] M. Kim, R. Fritschek, and R. F. Schaefer, "Learning End-to-End Channel Coding with Diffusion Models," *arXiv preprint arXiv:2309.10505*, Sep. 2023.
- [38] 3GPP TSG RAN WG1 "Evaluation on AI/ML for CSI feedback enhancement," Meeting #114, Toulouse, France, Tech. Rep., 21st August – 25th August 2023.